IEEE Open Journal of Vehicular Technology

Received 2 September 2024; accepted 25 September 2024. Date of publication 21 October 2024;
date of current version 5 November 2024. The review of this article was coordinated by Editor Derrick Wing Kwan Ng.

Digital Object Identifier 10.1109/OJVT.2024.3477268

Fairness-Aware Utility Maximization for Multi-UAV-Aided Terrestrial Networks

NISHANT GUPTA [1,2] (Member, IEEE), SATYAM AGARWAL [3] (Senior Member, IEEE), AND AYMEN FAKHREDDINE [4] (Member, IEEE)

[1]Department of Electrical Engineering, Linkoping University, 58183 Linköping, Sweden
[2]Department of Communications and Computer Engineering, The LNM Institute of Information Technology, Rajasthan 302031, India
[3]Department of Electrical Engineering, Indian Institute of Technology Ropar, Punjab 140001, India
[4]Institute of Networked and Embedded Systems, University of Klagenfurt, 9020 Klagenfurt, Austria

CORRESPONDING AUTHOR: AYMEN FAKHREDDINE (e-mail: aymen.fakhreddine@aau.at).

This work was supported by the Department of Science and Technology under Grant CRG/2020/005749. The work of Aymen Fakhreddine was supported by the Austrian Science Fund (FWF–Der Wissenschaftsfonds) under Grant ESPRIT-54 (Grant DOI: 10.55776/ESP54).

ABSTRACT Integrating unmanned aerial vehicles (UAVs) with terrestrial networks can enable high-speed communication in various applications. UAVs can serve as aerial base stations (ABSs), offering several benefits to the existing terrestrial networks, such as enhanced coverage, increased capacity, rapid deployment, and mobile communication support. However, this integration presents various technical challenges, including coordination, interference management, and dynamic allocation of resources. To address these key challenges, in this paper, we maximize the network utility by jointly optimizing the scheduling and cell association, transmit power of all base stations, and ABS deployment locations in the presence of co-channel interference. A two-stage approach is proposed to obtain a solution. In the first stage, we propose a heuristic solution by using the clustering algorithm to determine the initial ABS locations and user scheduling while ignoring the co-channel interference. In the second stage, we utilize the solution obtained in the first part and develop an interference-aware iterative scheme to jointly optimize user scheduling, resource allocation, and ABS placement. Given the non-convex nature of this problem, we employ the successive convex approximation technique to approximate the non-convex objectives and constraints. Numerical results show the proposed approach's insights and effectiveness over other schemes. Specifically, our proposed approach provides an average of 25% improvement over the benchmark schemes.

INDEX TERMS Integration of ABS-terrestrial network, joint scheduling and communication, downlink communication system, power allocation, and ABS deployment location.

I. INTRODUCTION

In recent years, there has been a notable surge in utilizing unmanned aerial vehicles (UAVs) as aerial base stations (ABSs) to cater to the communication needs of the users, particularly in scenarios such as rural areas, congested areas, hotspot areas, and so on [1]. This preference arises due to the challenges encountered by ground base stations (GBSs) in meeting the requirements of users, particularly in densely populated locales. Therefore, a UAV-aided communication system is seen as a new paradigm to improve the coverage of cellular communication [2], [3].

The integration of UAVs into communication networks as part of the infrastructure yields two distinct advantages. First, the inherent mobility of UAVs enables them to dynamically adjust to specific demands. Second, compared to fixed GBS, UAVs possess an inherent propensity to sustain line-of-sight (LoS) communication links with the users. While the UAV-aided communication system offers multiple advantages, deploying multiple UAVs introduces several challenges. First, in the UAV-aided communication system, pathloss not only depends on the users' locations but also the UAV's location. Secondly, handling the effects of co-channel interference on system throughput is more complicated than the conventional GBS because UAVs can fly in arbitrary directions [4].

In order to achieve efficient communication within a specific environment, the UAVs must operate in a coordinated

manner alongside the GBSs [5], [6]. This coordination between the UAVs and terrestrial networks can enable high-speed communication across a range of applications. Furthermore, it offers several benefits, such as enhanced coverage, increased capacity, rapid deployment, and mobile communication support. However, to enable the integration of UAVs with terrestrial networks, various technical challenges need to be addressed. These include scheduling and association of ground users between UAVs and terrestrial cells, effectively managing interference, optimizing power allocation, and strategically positioning UAVs following the prevailing system parameters.

To address these challenges, in this paper, we consider a UAV-aided terrestrial communication system, where multiple UAVs are deployed to assist the terrestrial network. We aim to maximize the network utility for the interference-limited communication system while jointly optimizing the user scheduling and association, power allocation, and deployment location of the UAVs. Such a setup is very useful in temporarily expanding the terrestrial network coverage area to support the additional ground users.

A. RELATED WORK

In the current decade, UAV-aided communication has gained considerable attention due to its various key attributes [7], [8]. With the growth in device numbers, a single UAV-assisted network may not provide enough communication and computation resources to satisfy the quality-of-service (QoS) requirement [9]. Therefore, researchers began to study the resource allocation for the multi-UAV-assisted systems. The authors in [10] developed an adaptive energy-efficient deployment scheme when multiple UAVs are deployed to serve the ground users. Furthermore, the authors in [11] maximized the minimum achievable throughput for all users by determining the location and transmit power of the multiple UAVs in the presence of co-channel interference. The authors in [12] studied the UAV deployment location and association schemes to minimize users' transmit power consumption in an uplink scenario. A recent work in [13] formulated a user satisfaction maximization problem to compute the multiple UAV locations and alleviate the overlapping coverage between UAVs to minimize inter-cell interference. Apart from the above works, several other works, such as [4], [14], consider the issue of co-channel interference and propose different methods to tackle them when considering multi-UAV aided networks.

Considering the potential of leveraging the computation and communication resources both in UAVs and the ground infrastructure, i.e., GBS, the aerial-ground cooperative paradigm is expected to enhance coverage and support the increasing data rate demand of smart applications in future wireless networks. Recent work in [15] proposed a heterogeneous multi-UAV-enabled collaborative aerial-ground framework for mobile edge computing. They maximized the total computation bits by optimizing the association, resources, and UAV trajectories. The authors in [16] studied the joint transmission of data from the UAVs and the GBS through the coordination of the software-defined network. The authors aim to maximize the network energy efficiency by jointly optimizing the UAV–user association, UAV location, resource allocation, and load allocation between the two systems. Furthermore, the authors in [17] studied the multiple UAV deployment framework for air-ground integrated networks. The authors maximized the number of covered users by user clustering and maximized the performance of users by jointly optimizing UAV trajectories and user scheduling.

Despite some recent efforts [15], [16], [17] devoted to investigating edge computing involving multiple UAVs and GBSs, there are still some challenges to be addressed. First, although multiple UAVs (or ABSs) are deployed to assist the communication service to the ground users, in practice, the coexisting of ABSs and GBSs will lead to severe co-channel interference. To this extent, the authors in [18] considered the co-channel interference that arises from the integration of UAVs with roadside units in vehicular networks; however, they propose that roadside units occupy the unlicensed spectrum and UAVs work on the licensed spectrum to alleviate the mutual interference. Second, spectrum reuse to support communications between multiple ABSs/GBS and users is needed to enhance spectrum efficiency and network performance. In this context, the authors in [14] have considered this issue but did not focus on the coexistence of the ABSs with the GBSs. Apart from the above two factors, it is essential to build a scheduling and resource allocation framework for cooperation between the ABSs and GBSs due to the limited resources available.

From the cellular-connected UAV perspective, The authors in [19] and [20] focused on cellular-connected UAV, examining inter-cell interference coordination (ICIC) techniques for a single UAV. They aimed to maximize the sum-rate of the UAV and all ground users in its ICIC region by jointly optimizing the UAV's cell association, resource block (RB) allocation, and transmit power. In [21], the authors studied uplink NOMA transmission from a single UAV and ground users to GBSs, maximizing sum rates by optimizing precoding vectors and mitigating interference with successive interference cancellation. Unlike [19], [20], [21], our work considers a cooperative framework between UAVs and GBSs in a downlink communication setup, UAVs act as ABSs, addressing co-channel interference and also incorporates user fairness constraint. This fairness constraint limits the optimizer to allocate the resources unevenly among users. A stringent fairness threshold pushes the optimizer to allocate the resources more evenly among users.

B. CONTRIBUTIONS

In this paper, we address the ABS deployment and its coexistence with GBS in an interference-limited scenario. We obtain the optimal user association and scheduling scheme to maximize network utility in terms of communication rate. This is achieved by jointly optimizing the user scheduling, power allocated to each user, and multi-ABS deployment location to mitigate interference effects. Moreover, we also

consider Jain's fairness index as a constraint, which helps identify underutilized channels and is not overly sensitive to typical network flow. The key contributions of this work are as follows:

- In comparison to the existing literature, this paper provides a cooperative framework between ABSs and GBSs by taking co-channel interference into account. This framework allows for a more integrated approach to manage interference, which is critical in dense network environments where both ABSs and GBSs operate on similar frequencies. By considering the co-channel interference between ABSs and GBSs, we provide a more realistic and effective deployment strategy.
- We formulate a utility maximization problem that optimizes the multi-ABS deployment location, user scheduling, and resources allocated to the ground users, subject to the constraints on user requirements and fairness. The inclusion of fairness constraint ensures that the network is not unduly benefited from the greedy users that have better channel gains compared to other users.
- Noting the non-convexity of the problem, we first propose a heuristic approach to have a low-complexity initialization. This heuristic approach leverages a clustering mechanism to provide a practical starting point. Subsequently, we propose an interference-aware iterative method to refine the initial solution and obtain a sub-optimal solution. This iterative approach takes into account the co-channel interference and adapts the deployment and resource allocation accordingly to improve network performance.
- Numerical results provide valuable insights into the effectiveness of our proposed approach. We highlight the performance improvements achieved through our method compared to conventional schemes. We also evaluate the solution obtained via different initialization schemes.

The organization of this paper is as follows. Section II presents the system model. Section III presents the problem definition. Sections IV and V present the proposed solution methodology, overall algorithm, and convergence analysis. Numerical results are plotted in Section VI, and finally, we conclude our work in Section VII.

II. SYSTEM MODEL

A. GENERAL MODEL

An interference-aware downlink communication setup in a multi-UAV-aided terrestrial network is described in Fig. 1, where multiple UAVs are deployed as ABSs to assist the GBS. The GBSs are indexed by $n \in \mathcal{N} \triangleq \{1, \ldots, N\}$, where N represents the number of GBS and the ABSs are indexed by $m \in \mathcal{M} \triangleq \{1, \ldots, M\}$, where M represents the number of ABS. Collectively, we denote $l \in \mathcal{L} \triangleq \{1, \ldots, N, N+1, \cdots N+M\}$ to represent the total number of BSs (i.e., GBSs and ABSs). The location of GBSs is fixed, while the location of m^{th}-ABS to be determined is given by $(\mathbf{q}_m, z_m)$, where

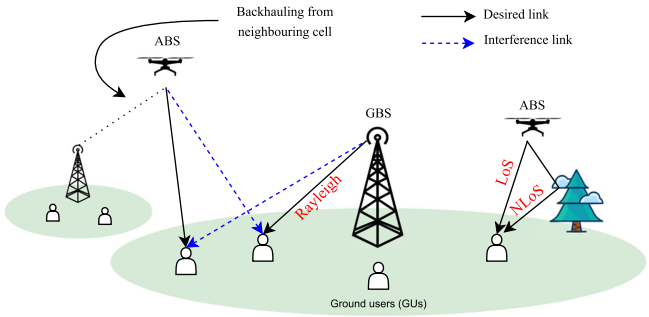

FIGURE 1. System model representing interference-aware downlink communication in heterogeneous networks.

$\mathbf{q}_m = [x_m, y_m]$, and z_m represent the lateral coordinates and altitude of the m^{th}-ABS, respectively. The ground users are indexed by $\mathcal{U} \triangleq \{1, \ldots, U\}$, and the location of the u^{th}-user is given by $\mathbf{w}_u$, where $\mathbf{w}_u = [x_u, y_u]$ represents the coordinate of u^{th}-user. We assume the location of users is known to the BSs (i.e., GBSs and ABSs), and the channel state information (CSI) is perfectly known to the BSs. In our setup, we assume the ABSs are provisioned with sufficient backhauling capacity from the GBS of the neighbouring cells. Furthermore, the consideration of the aerial users is kept as an extension of this work, where special attention is needed for antenna alignment and orientation.

B. CHANNEL MODEL

As shown in Fig. 1, the users undergo different channel conditions based on the type of BS. Users when connected to the GBSs experience a conventional ground-to-ground non-LoS (NLoS) fading link. This can be modelled as Rayleigh fading channel and is given by

$$h_{u,n} = \sqrt{\beta_{u,n}}\, \tilde{h}_{u,n}, \tag{1}$$

where $\beta_{u,n}$ is the large scale fading effects and $\tilde{h}_{u,n}$ is the Rayleigh small-scale fading with $\tilde{h}_{u,n} \sim \mathcal{CN}(0, 1)$. The large-scale fading effects can be expressed as

$$\beta_{u,n} = \beta_0 d_{u,n}^{-\bar{\alpha}}, \tag{2}$$

where β_0 is the pathloss at a reference distance of 1 m (m), $\bar{\alpha}$ is the pathloss exponent, and $d_{u,n}$ is the distance between the u^{th}-user and the n^{th}-GBS.

In practice, the users when connected to the ABSs receive three kinds of signals from the ABS, including LoS, NLoS, and multiple reflected signals. As discussed in [22], the probability of multipath fading caused by the multiple reflected signals is quite lower than the other two. Thus, we can ignore the effects of multiple reflected signals. Therefore, the channel between the user and the ABS follows the probabilistic LoS channel model. Under this assumption, the channel coefficient between the u^{th}-user and the m^{th}-ABS is given as

$$h_{u,m} = \sqrt{\beta_{u,m}}\, \tilde{h}_{u,m}, \tag{3}$$

where $\beta_{u,m}$ denotes the large-scale fading effects and $\tilde{h}_{u,m}$ denotes the small-scale fading effects, which is a complex-valued random variable with $\mathbb{E}[|\tilde{h}_{u,m}|^2] = 1$. The large-scale fading effects between the u^{th}-user and the m^{th}-ABS is modelled as a probabilistic LoS channel model, where the LoS and NLoS links occur with certain probabilities. Then $\beta_{u,m}$ can be written as

$$\beta_{u,m} = \begin{cases} \beta_0 d_{u,m}^{-\bar{\alpha}}, \text{ for LoS link, and} \\ \kappa \beta_0 d_{u,m}^{-\bar{\alpha}}, \text{ for NLoS link,} \end{cases} \tag{4}$$

where $\kappa < 1$ accounts for additional pathloss due to NLoS link. $d_{u,m}$ is the distance between the u^{th}-user and the m^{th}-ABS. The probability of having a LoS between the u^{th}-user and m^{th}-ABS is represented as

$$\mathcal{P}_{u,m}^{L} = (1 + c_1 \exp(-c_2[\phi_{u,m} - c_1]))^{-1}, \tag{5}$$

where c_1 and c_2 are the environmental parameters and $\phi_{u,m}$ is the elevation angle between the u^{th}-user and the m^{th}-ABS, which is given by $\phi_{u,m} = \frac{180}{\pi} \sin^{-1}\left(\frac{z_m}{d_{u,m}}\right)$. As a result, the channel power gain is given by

$$\begin{aligned} \mathbb{E}\left[|h_{u,m}|^2\right] &= \mathcal{P}_{u,m}^{L} \beta_0 d_{u,m}^{-\bar{\alpha}} + \left(1 - \mathcal{P}_{u,m}^{L}\right) \kappa \beta_0 d_{u,m}^{-\bar{\alpha}} \\ &= \widehat{\mathcal{P}}_{u,m}^{L} \beta_0 d_{u,m}^{-\bar{\alpha}}, \end{aligned} \tag{6}$$

where $\widehat{\mathcal{P}}_{u,m}^{L} = \mathcal{P}_{u,m}^{L} + \left(1 - \mathcal{P}_{u,m}^{L}\right) \kappa$.

C. DOWNLINK COMMUNICATION MODEL

We assume all the BSs share the same bandwidth, which is divided into K resource blocks (RBs), indexed by $k \in \{1, \ldots, K\}$. We define a binary variable $\alpha_{u,l}^{k} \in \{0, 1\}$, which shows that if the u^{th}-user is served by the l^{th}-BS in the k^{th}-RB, then $\alpha_{u,l}^{k} = 1$, otherwise $\alpha_{u,l}^{k} = 0$. In the k^{th}-RB, we consider every BS to be functional and provide communication service to only one ground user, i.e., total active connections in a RB is equal to the number of BSs. This assumption is particularly considered to limit the interference between the BSs and users in a single RB and to fully leverage the advantages of ABSs. Then, we have

$$\sum_{u=1}^{U} \alpha_{u,l}^{k} \leq 1, \forall k, l, \tag{7}$$

$$\alpha_{u,l}^{k} \in \{0, 1\}, \forall u, l, k. \tag{8}$$

Let $p_{u,l}^{k}$ be the power allocated to the u^{th}-user by the l^{th}-BS in the k^{th}-RB. Then, if u^{th}-user is served by l^{th}-BS, in the k^{th}-RB, then the SINR at u^{th}-user is given by

$$\gamma_{u,l}^{k} = \frac{p_{u,l}^{k} h_{u,l}}{\sum_{j \in \mathcal{L}, j \neq l} p_{u,j}^{k} h_{u,j} + \sigma^2}, \tag{9}$$

where $h_{u,l}$ represents the the channel between the u^{th}-user and the l^{th}-BS. $\sigma^2 = \frac{B}{K} N_0$, where B denotes the bandwidth and N_0 denotes the noise power spectral. The term $\sum_{j \in \mathcal{L}, j \neq l} p_{u,j}^{k} h_{u,j}$ in (9) denotes the co-channel interference caused by the other BSs in the k^{th}- RB. The interference generated in this particular scenario is illustrated in Fig. 1. For example, in the k^{th}-RB, three BS-user sets are active, then the other BSs apart from the desired will act as interferers.

Thus, the achievable data rate for the u^{th}-user in the k^{th}-RB is given by

$$R_u^{k} = \sum_{l=1}^{L} \alpha_{u,l}^{k} \frac{B}{K} \log_2\left(1 + \gamma_{u,l}^{k}\right). \tag{10}$$

Then, the sum rate of the u^{th}-user is given by

$$R_u = \sum_{k=1}^{K} \sum_{l=1}^{L} \alpha_{u,l}^{k} \frac{B}{K} \log_2\left(1 + \gamma_{u,l}^{k}\right). \tag{11}$$

III. PROBLEM FORMULATION

In this paper, we maximize the QoS or utility of the ground user when the ABSs are deployed in coexistence with GBSs in an interference-limited scenario. This is carried out by jointly optimizing the ABS deployment location, and user association and scheduling scheme to maximize network utility in terms of communication rate. In this section, we first define the utility function followed by the problem definition.

A. UTILITY FUNCTION

As multiple BSs are serving the ground users in a single RB and sharing the same frequency resources, the transmit power of one BS may bring additional interference to the users served by the other BSs. Moreover, the association factor and the ABS's location also affect the data rate of the ground users. Therefore, in the following, we aim to jointly optimize these three parameters. We define optimization variables as $\mathbf{A} = \{\alpha_{u,l}^{k}, \forall u, l, k\}$ represents the association policy between the BSs and the users, $\mathbf{P} = \{p_{u,l}^{k}, \forall u, l, k\}$ represents the transmit power and $\mathbf{Q} = \{(\mathbf{q}_m, z_m), \forall m \in \{1, \ldots, M\}\}$ represents the ABS deployment locations, where index u indicates the u^{th}-user, k indicate the k^{th}-resource block, and m indicates the m^{th}-ABS. Collectively, we denote $l \in \mathcal{L} \triangleq \{1, \ldots, N, N + 1, \cdots N + M\}$ to represent the total number of BSs (i.e., GBSs and ABSs). We define a utility function, where user QoS is measured and is given by

$$\mathcal{U}_u = \frac{1}{1 + \exp(-R_u)}, \tag{12}$$

which is considered to be a sigmoidal function based on the real-time requirements of the ground users [23], [24]. The benefit of employing a sigmoidal function lies in its ability to decrease their transmission rates up to a certain level, experiencing a graceful degradation in the QoS in response to the network congestion. However, decreasing the transmission rate below a certain threshold leads to a significant drop in the QoS. The elasticity of these services can be better described by using sigmoidal-like utility functions [23], [24]. Moreover, to ensure the fairness in terms of QoS experienced by users,

we introduce Jain's fairness index, which is given by

$$\frac{(\sum_{u=1}^{U} R_u)^2}{U \sum_{u=1}^{U} (R_u)^2} \geq J. \tag{13}$$

The above fairness index measures the fairness of a set of U users, and R_u is the throughput for the u^{th}-user [24]. The index ranges from $\frac{1}{U}$ (worst-case scenario) to 1 (best-case scenario). The index is set to its maximum value when all the users receive the same resource allocation. If $\tilde{U}$ users share equal resources, then the index is set to $\frac{\tilde{U}}{U}$, and the remaining $U - \tilde{U}$ users receive zero allocation, thus zero rate. The above fairness index is bounded by J to ensure that the greedy users are not unduly benefited. Thus, as the value of J increases, the number of users served by the network also increases, whereas a lower J value indicates fewer users being served.

B. PROBLEM DEFINITION

We maximize the system utility by jointly optimizing the user association $\mathbf{A}$, transmit power $\mathbf{P}$, and ABS deployment location $\mathbf{Q}$. The problem is formulated as

$$\text{P1}: \max_{\mathbf{A},\mathbf{P},\mathbf{Q}} \quad \sum_{u=1}^{U} \mathcal{U}_u,$$

$$\text{s.t.} \quad \frac{(\sum_{u=1}^{U} R_u)^2}{U \sum_{u=1}^{U} (R_u)^2} \geq J, \tag{14a}$$

$$\sum_{u=1}^{U} \alpha_{u,l}^{k} \leq 1, \forall l, k, \tag{14b}$$

$$\alpha_{u,l}^{k} \in \{0, 1\}, \forall u, l, k, \tag{14c}$$

$$\sum_{u=1}^{U} \alpha_{u,l}^{k} p_{u,l}^{k} \leq P_{max}^{l}, \forall k, l, \tag{14d}$$

$$\|(\mathbf{q}_m, z_m) - (\mathbf{q}_p, z_p)\| \geq D_{min}, \quad \forall m \neq p, m \in \{1, \ldots, M\}. \tag{14e}$$

where $\mathcal{U}_u$ is the utility of the u^{th}-user defined in (12). Constraint (14a) represents the fairness index as defined in (13). Constraints (14b) and (14c) represent the association constraints. In particular, (14c) is a binary constraint, and (14b) indicates that in a RB, each BS can serve at most one user, i.e., the number of users served in a RB is upper bounded by the number of BSs. Constraint (14d) limits the maximum transmit power of a l^{th}-BS in a RB to P_{max}^{l}. Finally, (14e) represents the collision avoidance constraint to ensure a minimum safe distance (D_{min}) between the ABSs.

Due to the non-concavity of $\gamma_{u,l}^{k}$ in (9), the objective function and constraint (14a) are non-convex. Furthermore, the sigmoidal nature of the utility function makes the objective function even more complex to tackle. Additionally, the constraint (14c) is an integer constraint. As a result, the problem P1 is a mixed-integer and non-convex programming problem. In the next subsections, we present the methodology to obtain a sub-optimal solution to P1.

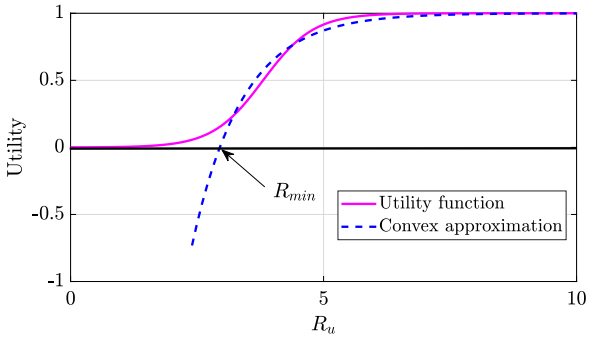

FIGURE 2. Convex approximation of utility function.

Remark 1: For static users, the deployment location of the ABSs is computed at once for all time steps. However, for mobile users, the optimization problem is a sub-routine to be solved in every time step, assuming that UAVs know users' location only at the beginning of every time step. Furthermore, the optimization problem needs to consider the remaining energy of the UAVs in the optimization problem so that the next location can be calculated in a way that allows the UAV to return to the charging station once its energy drops below the threshold.

C. APPROXIMATION OF UTILITY FUNCTION

Since the utility function $\mathcal{U}_u$ is non-convex, we first present the convex approximation to this function, which is given by [24]

$$\mathcal{U}_u^a = 1 - \exp(-c_4 R_u), \tag{15}$$

where c_4 is a constant. The above function is concave concerning R_u and indicates that before a particular value of R_u, the utility is negative, whereas in the original function, it is close to zero as shown in Fig. 2. The approximate function closely matches the sigmoid function when $R_u > R_{min}$, where R_{min} is the minimum requested rate by each user. However, for $R_u < R_{min}$, its value is negative, which serves as a penalty, indicating that the rate cannot be lower than R_{min}. If, for a particular user, it's $\mathcal{U}_u^a$ turns out to be negative after optimization, it is better to drop the user as the network cannot support the minimum data rate requirement of that user. Thus, in that case, $\mathcal{U}_u^a = 0$.

To simplify (15) further, we present the following proposition

Proposition 1: Using $\widehat{\mathcal{U}}_u = c_4 R_u$ instead of $\mathcal{U}_u^a$ in problem P1 is equivalent if $R_u > R_{min}, \forall u \in \mathcal{U}$.

Proof: Using $e^{-a} \approx 1 - a, \forall a \ll 1$, in (16), and since the $\mathcal{U}_u^a$ is a strictly increasing function of R_u, the two optimization problems with objective functions $\widehat{\mathcal{U}}_u = c_4 R_u$ and $\mathcal{U}_u^a = 1 - \exp(-c_4 R_u)$ are equivalent and share the same set of optimal points $(\mathbf{A}^*, \mathbf{P}^*, \mathbf{Q}^*)$ [25]. Though optimal values are different but they are related as

$$\mathcal{U}_u^{a*} = 1 - \exp(-\widehat{\mathcal{U}}_u^*), \tag{16}$$

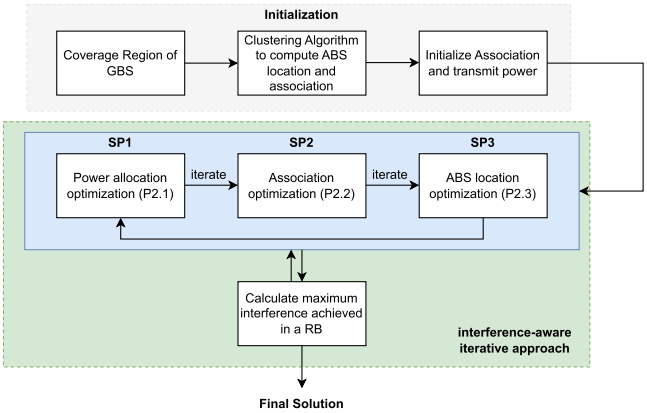

FIGURE 3. Low-complexity proposed approach to obtain a solution to P2.

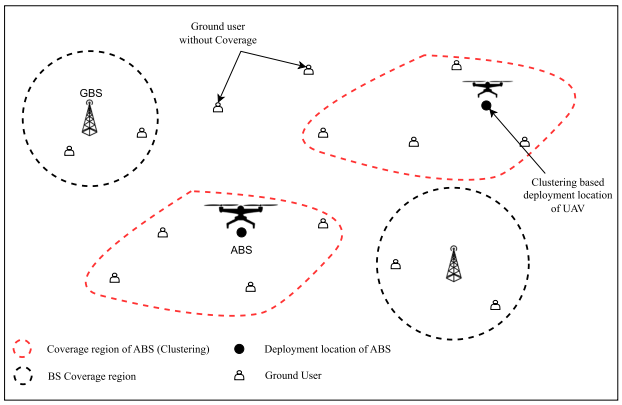

FIGURE 4. Two-dimensional (2D) view of the proposed initialization scheme.

Thus, the solution obtained by maximizing this simplified $\widehat{\mathcal{U}}_u$, can be applied to the maximization of $\mathcal{U}_u^a$ by relating them according to (16). ■

Accounting for the above proposition, P1 can be re-written as

$$\text{P2}: \max_{\mathbf{A},\mathbf{P},\mathbf{Q}} \quad \sum_{u=1}^{U} \widehat{\mathcal{U}}_u,$$

$$\text{s.t.} \quad (14a) - (14e).$$

D. PROPOSED SOLUTION METHODOLOGY

It is worth highlighting that problem P2 is still non-convex. The main difficulty lies in managing the interference caused by the presence of other BSs, making the problem complex and difficult to solve analytically. To address this issue, we divide our proposed methodology into two parts. In the first part, we propose a heuristic solution based on the clustering-based placement of the ABSs ignoring the interference generated by the other BSs as the initialization step. In the second part, we propose an iterative approach that aims to tackle the interference issue. It involves an iterative process designed to minimize interference in every successive iteration. In other words, in the first part, we start by initializing the user scheduling and association, power allocated to each user, and the deployment location of the ABSs while assuming there is no interference. Subsequently, we analyze the potential maximum interference that could occur within a RB based on the first part. Thereafter, we solve Problem P2, where we treat $P_{I,k} \triangleq \sum_{j\in\mathcal{L}, j\neq l} p_{u,j}^k h_{u,j}$ in (9) to be fixed equal to the maximum interference obtained. The problem P2 is solved until the interference between the two consecutive iterations is below a predefined threshold. This approach is named as *interference-aware iterative approach*. In this way, we can effectively mitigate the interference effects caused by other serving BSs, resulting in an improved solution for problem P2. The proposed solution is briefly described in Fig. 3.

In the subsequent sections, we describe each of the two parts in more detail.

IV. INITIALIZATION

In this section, we propose a heuristic approach used as an initialization scheme to solve problem P2. In particular, we utilize the clustering mechanism to compute the deployment location of the ABSs and then obtain a solution for user scheduling and power allocation. We divide this approach into three sequential steps, namely, coverage region, clustering, and initialization, described briefly as follows.

1) Coverage Region: We divide the coverage region into two regions: the GBS-occupied region and the GBS non-occupied region. The GBS-occupied region is designed to ensure that the GBS delivers a higher data rate compared to the ABS, even when the ABS is located within this area. This benefit arises due to the differing transmit power levels of these base stations. The illustration of the GBS-occupied region around the GBS is shown in Fig. 4 by black dotted circles. The rest of the region is referred to as the GBS non-occupying region.

2) Clustering: After determining the GBS-occupied region, the next step involves ensuring coverage for users located in the GBS non-occupied region by strategically placing the ABSs. In this GBS non-occupied region, ABSs may offer the advantage of potentially delivering higher data rates than the GBS. This enhanced performance arises from the ABSs' ability to be deployed more flexibly. Since the channel capacity decreases with an increase in the distance, the cluster users are as close as possible to their assigned ABS [26]. Thus, we employ a clustering mechanism (particularly, k-means clustering) to compute the association index of the ground users with the ABSs, provided the ABS deployment location is computed using the clustering algorithm. This algorithm groups the users in the GBS non-occupied regions into clusters equal to the available number of ABSs and produces a centroid for each cluster. Then, the ABS is deployed at each cluster at the prescribed altitude. Although the algorithm may not yield an optimal solution, its performance remains fairly competitive with advanced placement algorithms [26].

3) Initialization: Once the initial location of the ABSs and the users associated with the ABSs is known, we

next initialize the association policy $\mathbf{A}$ and find the $\mathbf{A}^{ini} = \{\alpha^k_{u,m}, \forall u, m, k\}$. Thereafter, we assume that the ABS allocates equal power to its associated ground user, which is denoted by $\mathbf{P}^{ini} = \{p^k_{u,m}, \forall u, m, k\}$.

By employing the above approach, we can intelligently initialize $\mathbf{A}$, $\mathbf{P}$, and $\mathbf{Q}$, which satisfies all the constraints. However, we cannot solely depend on the above heuristic due to our assumption of frequency reuse across RBs. While this method is highly valuable for initialization purposes, it may not fully address the complexities introduced by interference among BSs. Therefore, while it serves as an effective starting point, additional strategies are necessary to address interference-related challenges as we proceed with the optimization process.

V. INTERFERENCE-AWARE ITERATIVE APPROACH

Since the joint optimization of scheduling, power, and ABS location in the second part leads to a mixed-integer non-convex programming problem, we decompose Problem P2 into three subproblems. In the first subproblem (SP1), we optimize the transmit power allocation for the given user association matrix and ABS locations. In the second subproblem (SP2), we optimize the user association for a given power allocated by the BSs to the ground user and for a given location of ABSs. Finally, in the third subproblem (SP3), we obtain the optimal deployment location based on the previously obtained association and power allocation. The above three subproblems are solved successively until the converged solution is achieved. Note that the solution of SP1, SP2, and SP3 considers fixed interference, that is, in (9), we treat $P_{I,k} \triangleq \sum_{j\in\mathcal{L}, j\neq l} p^k_{u,j}\, h_{u,j}$ to be fixed while solving P2. Next, we discuss each of the subproblems in detail followed by the overall algorithm and the convergence analysis.

A. SP1: POWER OPTIMIZATION

For a given $\mathbf{Q}$ and $\mathbf{A}$, the problem to obtain $\mathbf{P}$ is given as

$$\text{P2.1}: \max_{\mathbf{P}} \quad \sum_{u=1}^{U} \widehat{\mathcal{U}}_u,$$
$$\text{s.t.} \quad \text{(14a), (14d).}$$

Following the definition of $\widehat{\mathcal{U}}_u$, we have

$$\widehat{\mathcal{U}}_u = c_4 \sum_{k=1}^{K} \frac{B}{K} \left[\sum_{n=1}^{N} \alpha^k_{u,n} \log_2\left(1+\gamma^k_{u,n}\right) + \sum_{m=1}^{M} \alpha^k_{u,m} \log_2\left(1+\gamma^k_{u,m}\right) \right]. \tag{17}$$

It can be easily observed that the objective function $\widehat{\mathcal{U}}_u$ is concave with respect to $\mathbf{P} = \{p^k_{u,l}, \forall u, l, k\}$ and the constraint (14d) is linear. However, (14a) is a non-convex constraint. To tackle this constraint, we re-arrange it into a more appropriate form, expressed as

$$\sqrt{J.U} \sqrt{\sum_{u=1}^{U} (R_u)^2} \leq \sum_{u=1}^{U} R_u. \tag{18}$$

To ensure that (18) is convex, we need to show that the left side of the inequality exhibits convex behaviour while the right side is concave. From R_u defined in (11), it can be observed that R_u is concave in $\mathbf{P}$, since logarithm preserves the concavity. Thus, the right side of the inequality is concave. However, the left side of the inequality is non-convex. Even though square root preserves the convexity [27], $(R_u)^2$ is non-convex due to the concavity of R_u. Thus, we take the first-order Taylor series expansion of R_u with respect to $\mathbf{P}$, and we get

$$\log_2\left(1+\mathcal{A}_1 p^{k,r}_{u,l}\right) + \frac{\mathcal{A}_1 (p^k_{u,l} - p^{k,r}_{u,l})}{1+\mathcal{A}_1 p^{k,r}_{u,l}} \leq R^{lb}_u, \tag{19}$$

where $\mathcal{A}_1 = \frac{h_{u,l}}{P_{I,k}+\sigma^2}$. Then, using (19), (18) can be approximated as

$$\sqrt{J.U} \sqrt{\sum_{u=1}^{U} \left(R^{lb}_u\right)^2} \leq \sum_{u=1}^{U} R_u, \tag{20}$$

which is now a convex constraint. As a result, P2.1 is now a convex optimization problem.

B. SP2: USER ASSOCIATION

For a given $\mathbf{Q}$ and $\mathbf{P}$, the problem to obtain $\mathbf{A}$ is given as

$$\text{P2.2}: \max_{\mathbf{A}} \quad \sum_{u=1}^{U} \widehat{\mathcal{U}}_u,$$
$$\text{s.t.} \quad \text{(18), (14b)}-\text{(14d).}$$

The objective function, and constraints (18), (14b), and (14d) are all convex. However, the above problem is non-convex due to the binary variable $\alpha^k_{u,l}$ in (14c). Thus, to handle (14c), we convert the binary into the continuous variable, where $0 \leq \alpha^k_{u,l} \leq 1$. As a result, P2.2 is now a convex optimization problem.

C. SP3: ABS DEPLOYMENT LOCATION

For a given $\mathbf{A}$ and $\mathbf{P}$, the problem to obtain $\mathbf{Q}$ is given as

$$\text{P2.3}: \max_{\mathbf{Q}} \quad \sum_{u=1}^{U} \widehat{\mathcal{U}}_u,$$
$$\text{s.t.} \quad \text{(18), (14e).}$$

The above problem is non-convex since the objective function and constraints (18), and (14e) depend on the ABS location not only through the distance between the user and the ABS but also via the probabilistic LoS channel. Moreover, in $\widehat{\mathcal{U}}_u$ (defined in (17)), only $\gamma^k_{u,m}$ depends on the ABS location. Thus, to make $\widehat{\mathcal{U}}_u$ concave, we introduce an auxiliary

Algorithm 1: Iterative Approach to Obtain $\mathbf{A}$, $\mathbf{P}$, and $\mathbf{Q}$ for Fixed Interference.

Require: A^{ini}, P^{ini}, Q^{ini}, $P_{I,k}$.
1: Initialize $\mathbf{A}^0 = A^{ini}$, $\mathbf{P}^0 = P^{ini}$, and $\mathbf{Q}^0 = Q^{ini}$. Set iteration number $r = 0$, and acceptable tolerance ϵ.
2: **Repeat**
3: Fix $\mathbf{A}^r$, $\mathbf{Q}^r$ and solve for $\mathbf{P}^{r+1}$ in Problem P2.1.
4: Fix $\mathbf{P}^{r+1}$, $\mathbf{Q}^r$ and solve for $\mathbf{A}^{r+1}$ in Problem P2.2.
5: Fix $\mathbf{A}^{r+1}$, $\mathbf{P}^{r+1}$, initialize $i = 0$, $\mathbf{q}_m^i = \mathbf{q}_m^r$, and $z_m^i = z_m^r$,
6: **Repeat**
7: Fix z_m^i and solve for $\mathbf{q}_m^{i+1}$ in P2.3b.
8: Fix $\mathbf{q}_m^{i+1}$ and solve for z_m^{i+1} in P2.3c.
9: Set $i = i + 1$, and calculate $\sum_{u=1}^{U} \widehat{\mathcal{U}}_u^{i+1}$
10: **Until** $\sum_{u=1}^{U} \widehat{\mathcal{U}}_u^{i+1} - \sum_{u=1}^{U} \widehat{\mathcal{U}}_u^{i} \leq \epsilon$.
11: Set $\mathbf{Q}^{r+1} = [\mathbf{q}_m^{i+1}, z_m^{i+1}]$ and update $\{\mathbf{A}^r, \mathbf{P}^r, \mathbf{Q}^r\}$ with $\{\mathbf{A}^{r+1}, \mathbf{P}^{r+1}, \mathbf{Q}^{r+1}\}$.
12: Set $r = r + 1$, and calculate $\sum_{u=1}^{U} \widehat{\mathcal{U}}_u^{r+1}$.
13: **Until** $\sum_{u=1}^{U} \widehat{\mathcal{U}}_u^{r+1} - \sum_{u=1}^{U} \widehat{\mathcal{U}}_u^{r} \leq \epsilon$.

variable $b_{u,m}^k$ such that

$$b_{u,m}^k \leq \frac{(1-\kappa)\mathcal{P}_{u,m}^L + \kappa}{\|\mathbf{q}_m - \mathbf{w}_u\|^2 + z_m^2}. \tag{21}$$

Then, $\gamma_{u,m}^k$ can be written as

$$\gamma_{u,m}^k = \frac{p_{u,m}^k b_{u,m}^k}{P_{I,k} + \sigma^2}, \tag{22}$$

which is now concave with respect to $b_{u,m}^k$ and so is $\widehat{\mathcal{U}}_u$. However, there is an addition of additional non-convex constraint (21) in the optimization problem P2.3. Next, we introduce the following lemma that rewrites (21) into an equivalent and simpler form.

Lemma 1: The non-convex constraint (21) can be represented by constraints (30)–(34) (shown in Appendix A). The constraint (21) is equivalent to (30)–(34).

Proof: See Appendix A. ∎

Then, utilizing Lemma 1, problem P2.3 is transformed into

$$\text{P2.3a}: \max_{\mathbf{Q},\mathcal{X}} \quad \sum_{u=1}^{U} \widehat{\mathcal{U}}_u,$$
$$\text{s.t.} \quad (18), (14e), (30) - (34)$$

where $\mathcal{X} = \{b_{u,m}^k, \beta_{u,m}^k, y_{u,m}^k, \Theta_{u,m}^k\}$. In the above problem, the constraint (18), (14e), (30), (32), and (33) are all non-convex constraints.

To maintain the analytical tractability, we divide P2.3a into two parts: Lateral coordinate optimization ($\mathbf{q}_m$) and altitude optimization (z_m).

1) LATERAL COORDINATE OPTIMIZATION

Note that the constraints, (18), (14e), (30), (32), and (33) are still non-convex with respect to $\mathbf{q}_m$. Therefore, we first follow the procedure to convexify the non-convex constraints.

Lemma 2: The constraint presented in (32) can be reformulated into a convex expression as

$$\frac{1}{2}\left(\Theta_{u,m}^k + \|\mathbf{q}_m - \mathbf{w}_u\|\right)^2 - \lambda_{u,m}^k \leq z_m, \tag{23}$$

where $\lambda_{u,m}^k$ is given in (36).

Proof: See Appendix B. ∎

Following the same procedure as defined in Lemma 2, (33) can be approximated as

$$P_{\Theta_{u,m}^k} - \left(\frac{1}{y_{u,m}^{k,r}} + \frac{(y_{u,m}^k - y_{u,m}^{k,r})}{(y_{u,m}^{k,r})^2}\right) \leq 0, \tag{24}$$

where $P_{\Theta_{u,m}^k} = 1 + c_1 \exp(-c_2[\tan^{-1}\Theta_{u,m}^k - c_1])$. Similarly, (30) can be approximated as

$$\frac{1}{2}\left(b_{u,m}^k + \|\mathbf{q}_m - \mathbf{w}_u\|^2\right)^2 + b_{u,m}^k z_m^2 - \Gamma_{u,m}^k \leq \beta_{u,m}^k, \tag{25}$$

where $\Gamma_{u,m}^k = \frac{1}{2}((b_{u,m}^{k,r})^2 + \|\mathbf{q}_m^r - \mathbf{w}_u\|^4) + b_{u,m}^{k,r}(b_{u,m}^k - b_{u,m}^{k,r}) + \|\mathbf{q}_m^r - \mathbf{w}_u\|^2(\|\mathbf{q}_m - \mathbf{w}_u\|^2 - \|\mathbf{q}_m^r - \mathbf{w}_u\|^2)$. As a result of the above transformation, the constraints, (30), (32), and (33) are now convex. Since the above procedure is followed to deal with the non-convexity of $\gamma_{u,m}^k$ by introducing the auxiliary variable, the same is also valid for constraint (18). Next, the non-convex constraint (14e) can be easily converted into the convex constraint, by following [28, Eq. (29)].

Taking into consideration the preceding discussion and Lemmas 1-2 to transform the constraints into convex forms, it can be seen that problem P2.3a when expressed in lateral coordinates, can be approximated as a convex problem (named P2.3b). Consequently, we can employ the interior point method to devise the solution. Leveraging the first-order Taylor expansion to establish bounds on the non-convex constraints, the approximate problem P2.3b can be viewed as a subset of the original problem P2.3a in lateral coordinates.

2) ALTITUDE OPTIMIZATION

Concerning z_m, the problem is non-convex due to constraints (18), (33), and (30) which are non-convex and the non-concave objective function.

Using the same techniques as described for the lateral coordinate subproblem, we can transform the constraint (33) to a convex constraint as given in (24). Similarly, we can rewrite (30) in convex form as

$$\frac{1}{2}\left(b_{u,m}^k + z_m^2\right)^2 + b_{u,m}^k \|\mathbf{q}_m - \mathbf{w}_u\|^2 - \Gamma_{u,m}^k \leq \beta_{u,m}^k, \tag{26}$$

where $\Gamma_{u,m}^k = \frac{1}{2}((b_{u,m}^{k,r})^2 + (z_m^r)^4) + b_{u,m}^{k,r}(b_{u,m}^k - b_{u,m}^{k,r}) + (z_m^r)^2(z_m^2 - (z_m^r)^2)$. Considering the application of the first-order Taylor expansion, the problem P2.3a in z_m (named P2.3c) is now a convex problem and can be solved using the interior point method. Similar to the lateral coordinate subproblem, P2.3c also converges to a locally optimal solution.

Algorithm 2: Overall Algorithm.

Require: N, M, location of GBSs, and location of users.
1: Compute the GBS-occupied coverage region.
2: Apply k-means clustering approach on the users present in the GBS non-occupying region based on the available ABSs to obtain the location of the ABSs and initialize A^{ini}, P^{ini}, Q^{ini}.
3: Set acceptable tolerance ϵ_I, and iteration count $r = 0$.
4: Calculate $P^r_{I,k}$ by using A^{ini}, P^{ini}, Q^{ini}.
5: **repeat**
6: Call Algorithm 1 to obtain $\{\mathbf{A}^r, \mathbf{P}^r, \mathbf{Q}^r\}$.
7: Set $r = r + 1$, and calculate $P^{r+1}_{I,k}$ from $\{\mathbf{A}^{r+1}, \mathbf{P}^{r+1}, \mathbf{Q}^{r+1}\}$.
8: **Until** $P^{r+1}_{I,k} - P^r_{I,k} \leq \epsilon_I$.

Thereafter, by solving the lateral and altitude optimization subproblems, i.e., P2.3b, and P2.3c, respectively, we can determine the sub-optimal deployment locations of ABSs represented by $\mathbf{Q}$ for a given association $\mathbf{A}$ and power allocation $\mathbf{P}$. In the first stage, we find $\{\mathbf{q}_m, \forall m\}$ with a fixed $\{z_m, \forall m\}$. In the second stage, we find $\{z_m, \forall m\}$ with the obtained $\{\mathbf{q}_m, \forall m\}$. These two stages are performed iteratively until the difference in the objective function is below a certain pre-defined threshold, indicating convergence.

D. OVERALL ALGORITHM

Algorithm 1 shows the steps to solve P2 for a given $P_{I,k}$. Particularly, in step 3, at r^{th}-iteration, for any given $\mathbf{A}^r$ and $\mathbf{Q}^r$, we optimize the power allocated to each user. In step 4, for an optimized power $\mathbf{P}^{r+1}$, we optimize the $\mathbf{A}^{r+1}$ scheduling vector, and finally, in steps 5–10, the ABS locations $\mathbf{Q}^{r+1}$ are optimized by solving the lateral and altitude optimization subproblems successively. Finally, Algorithm 1 returns the optimized $\mathbf{A}^*$, $\mathbf{P}^*$, and $\mathbf{Q}^*$ that maximizes the network utility.

Since Algorithm 1 returns the solution to P2 for a given $P_{I,k}$, we present an interference-aware iterative approach to obtain a sub-optimal solution while accounting for interference. We outline the complete algorithm in Algorithm 2. In step 1-2, we initialize the scheduling $\mathbf{A}^{ini}$, power $\mathbf{P}^{ini}$, and ABS's location $\mathbf{Q}^{ini}$ as described in Section IV. In step 3, we calculate the interference generated in a RB and then set $P_{I,k}$ equal to the maximum interference that is achieved in a RB. Utilizing this $P_{I,k}$, steps 4 to 7 correspond to solving P2 for a given $P_{I,k}$ using Algorithm 1. The algorithm continues to run until it finds a solution where the objective function in two successive iterations is less than a pre-defined tolerance ϵ_I.

E. COMPLEXITY AND CONVERGENCE ANALYSIS

The overall complexity of the proposed approach depends on solving the non-convex problems, i.e., scheduling, power, and location optimization subproblems. In particular, it depends on Algorithm 1 where these three subproblems are solved iteratively. On one hand, the complexity to solve problem P2.1 and P2.2 is given by $C_{ap} \triangleq \mathcal{O}((KU(M+N))^{3.5}\log(1/\epsilon))$. On the other hand, the complexity to solve P2.3b and P2.3c is given by $C_q \triangleq \mathcal{O}((4KUM + M)^{3.5}\log(1/\epsilon))$, where $4KUN + M$ represents the number of optimization variables and ϵ represents the required accuracy of the obtained solution [29]. Let L_{iter} indicate the number of iterations to achieve convergence of Algorithm 1 and L_{P_l} indicate the number of iterations to achieve an interference less than a pre-defined tolerance ϵ_I in Algorithm 2, respectively. Then, the overall complexity is given by $\mathcal{O}(L_{iter}L_{P_l}\max(C_{ap}, C_q))$.

To verify the convergence of our proposed approach, it is necessary to demonstrate the convergence of the alternating optimization approach used in Algorithm 1. It is worth noting that as explained in [30], the alternating optimization converges whenever a convex optimization problem is solved in each iteration. Thus, the convergence of our proposed approach depends on the convergence of SP1, SP2, and SP3 (i.e., Algorithm 1). Since we have utilized the successive convex approximation approach to approximate the problem into the convex problem, we need to show that the value of the objective function increases in each iteration for a maximization problem to verify convergence.

We define $R(\mathbf{H}, \mathbf{Z})$, and $R^{lb}_{hor}(\mathbf{H}, \mathbf{Z})$, as the objective value of P2, and problem P2.3b (lateral optimization), respectively, with $\mathbf{H} = \{\mathbf{q}_m, \forall m\}$ and $\mathbf{Z} = \{z_m, \forall m\}$. For a fixed $\mathbf{Z}^r$, $\mathbf{H}^{r+1}$ is optimized by solving P2.3b. Then, we have

$$\begin{aligned} R(\mathbf{H}^r, \mathbf{Z}^r) &\overset{(a)}{=} R^{lb}_{hor}(\mathbf{H}^r, \mathbf{Z}^r) \\ &\overset{(b)}{\leq} R^{lb}_{hor}(\mathbf{H}^{r+1}, \mathbf{Z}^r) \\ &\overset{(c)}{\leq} R(\mathbf{H}^{r+1}, \mathbf{Z}^r), \end{aligned} \tag{27}$$

where (a) is obtained by using the first-order Taylor expansion of the constraints at the local point, and thus (a) is valid. (b) holds since the $\mathbf{H}^{r+1}$ is the optimal solution of the approximated maximization problem with the given $\mathbf{Z}^r$ after applying the Taylor-first order expansion, and (c) holds because the approximate problem is the lower bound of the original problem at $\mathbf{H}^{r+1}$. Consequently, it can be inferred from (27) that the objective function after each iteration is non-decreasing. As a similar procedure is followed to obtain $\mathbf{Z}$ from P2.3c, then we have

$$R(\mathbf{H}^{r+1}, \mathbf{Z}^r) \leq R(\mathbf{H}^{r+1}, \mathbf{Z}^{r+1}). \tag{28}$$

From (27) and (28), we can easily obtain $R(\mathbf{H}^r, \mathbf{Z}^r) \leq R(\mathbf{H}^{r+1}, \mathbf{Z}^{r+1})$. It indicates that the objective value for Step 6 to Step 10 of Algorithm 1 either increases or stays the same after each iteration when solving both the lateral and altitude optimization subproblems. Therefore, SP3 guarantees convergence. Similar explanation is also applicable to SP1.

Since we have followed the alternating optimization approach in Algorithm 1 to obtain $\mathbf{A}^{r+1}$, $\mathbf{P}^{r+1}$ and $\mathbf{Q}^{r+1}$, then

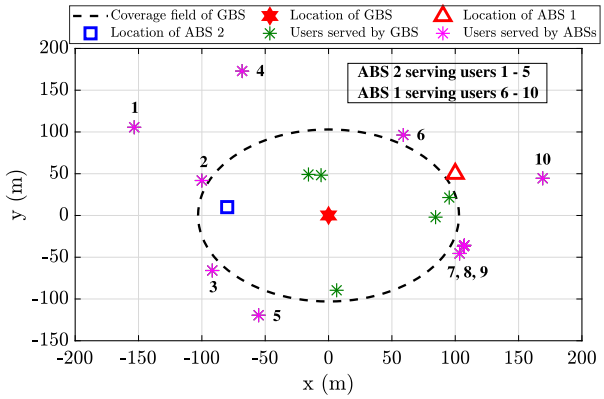

FIGURE 5. Illustration of network initialization in 2D.

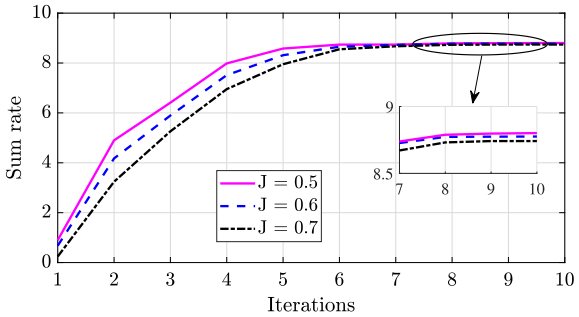

FIGURE 6. Convergence of proposed approach.

we can directly write

$$R(\mathbf{A}^r, \mathbf{P}^r, \mathbf{Q}^r) \leq R\left(\mathbf{A}^{r+1}, \mathbf{P}^{r+1}, \mathbf{Q}^{r+1}\right). \tag{29}$$

This shows that Algorithm 1 guarantees convergence.

VI. RESULTS AND DISCUSSIONS

In this section, we present the numerical results to show the proposed approach's performance and effectiveness over the benchmark schemes. The simulation parameters are given as follows. The maximum transmit power of ABS is taken as $P^m_{max} = 10$ Watts (W) [31], and that of GBS is taken as $P^n_{max} = 40$ W [32]. The other parameters are given as $B = 1$ MHz, $\bar{\alpha} = 2.5$, $c_1 = 10$, $c_2 = 0.6$, $\kappa = 0.2$. The same numerical values are considered to get insights into the system performance unless specified.

A. PROPOSED INITIALIZATION

To illustrate the initialization scheme, we plot Fig. 5 for a typical scenario, where one GBS, i.e., $N = 1$ is present at location (0,0,15), and $M = 2$ ABSs are present to provide the communication service. We assume $U = 15$ ground users are present in the described area, and the number of RBs is $K = 5$. Given the system settings, in Fig. 5, the black dotted circle shows the coverage area of GBS, wherein the rate achieved by each user from the GBS is always higher than that of ABS, even if the ABS when present inside the circular region transmits at P^m_{max}. Note that we do not take into account the interference in our initialization scheme; thus, the black dotted circle does not account for interference. As a result, the users present inside the black dotted circle are served by the GBS. Then, to provide coverage to the rest of the users, we applied the K-means clustering algorithm to find the location of the ABSs and their association when the ABSs transmit with fixed transmit power, as described in Section IV [33]. Fig. 5 also shows the ABS's location and the users associated with each ABS. Here, users 1-5 are associated with ABS 2, and users 6-10 are associated with ABS 1.

B. PERFORMANCE ANALYSIS

For the above setup and initialization, we first study the convergence of the proposed approach and its performance insights in this subsection. Fig. 6 shows the convergence of the proposed approach and the number of iterations required to reach the converged solution for different values of fairness index $J = \{0.5, 0.6, 0.7\}$. The iteration number indicates the number of times P2.1, P2.2, and P2.3 are solved iteratively to obtain the sub-optimal solution. Fig. 7 illustrates the users' association with each BS across each RB using the proposed approach. Furthermore, Fig. 7 shows the deployment location of the ABSs when the network utility is maximized with fairness index $J = 0.5$. Two important aspects are highlighted. First, the ABS 2 predominantly provides communication service to the users that were initially associated during the initialization, for example, users $\{1, 2, 4\}$ from the existing set $\{1, 2, 3, 4, 5\}$. Correspondingly, ABS 1 serves users $\{6, 8\}$ from the existing set $\{6, 7, 8, 9, 10\}$. Secondly, the farthest users, for example, users $\{5, 10\}$, which were initially associated with ABSs, remain unserved. This implies for $J = 0.5$, the network lacks the capacity to accommodate all the users. This implies we need to increase the fairness index J to ensure that the user is covered in the network.

To show the capability of the network to support all the ground users, we plot Fig. 8 for different values of fairness index J. The fairness constraint restricts the optimizer from allocating resources unevenly among users. When the fairness threshold is set higher, the optimizer is driven to distribute resources more equally among users. As a result, it can be observed that as the fairness index increases, the optimizer tries to allocate power to the users that were previously not served, thus increasing the fairness while at the same time decreasing the network utility and the sum rate. Moreover, the minimum utility is achieved when $J = 0.8$ for $K = 5$ and after this value, the network is not able to satisfy the fairness constraint. Note that this value typically depends on the users' distribution and thus can vary. Moreover, it can be seen from Fig. 7 that when $J = 0.5$, some users have multiple coverages, i.e., the ground users are scheduled in different RBs which implies the user can connect to different BSs in different RBs.

To get a deeper insight into the solution obtained by the proposed approach, we plot Fig. 9(a) and (b). Specifically, these

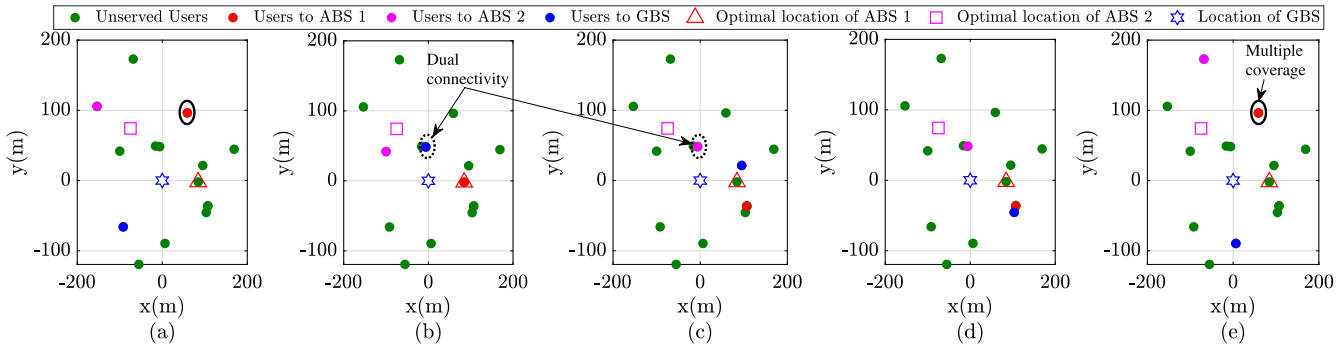

FIGURE 7. Association of the ground user to BSs in each RB (a) RB 1, (b) RB 2, (c) RB 3, (d) RB 4, and (e) RB 5.

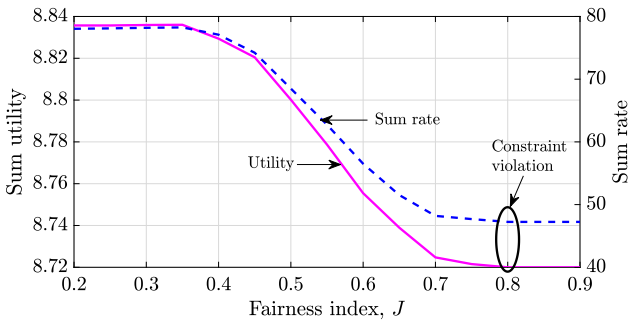

FIGURE 8. Network utility as a function of fairness constraint J.

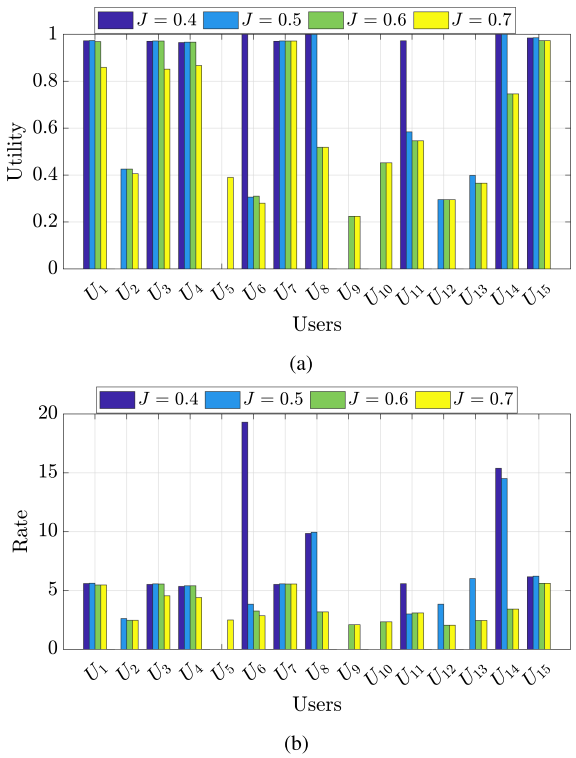

FIGURE 9. (a) Utility, and (b) rate of each ground user for different fairness index.

figures show the utility and data rate attained by individual ground users considering four distinct fairness index values, $J = \{0.4, 0.5, 0.6, 0.7\}$. Case 1 ($J = 0.4$): At $J = 0.4$, it can be observed that the optimizer is unable to provide service to many ground users, for example, users $\{2, 5, 9, 10, 12, 13\}$. This is because the focus is to maximize the utility, and all these users are either far away or experience bad channel conditions. Case 2 ($J = 0.5$): As we indicated above, the inclusion of fairness constraint prevents the greedy users from occupying all the resources from the BSs; the same can also be observed in Fig. 9(a) and (b). The users who were earlier not provided communication are now covered by the BSs. Though the utility/rate of those users is less, they still have network connectivity. Out of all the users present in the network, now $\{5, 9, 10\}$ remains unserved. Case 3 ($J = 0.6$): When J is further increased, more users can now be accommodated to satisfy the fairness constraint. As a result, only user 5 is left unserved by the network. A further increase in J will result in the association of user 5. For instance, Case 4 ($J = 0.7$): Increasing J to $J = 0.7$ led to the inclusion of user 5. It is important to note that a fairness index of $J = 0.7$ does not imply that all users will have nearly identical rates, but ensures that every user is covered. Furthermore, as J continues to rise, the rates of all users become more comparable, albeit at the expense of reducing the overall network utility.

C. PERFORMANCE COMPARISON

To verify the performance of the proposed scheme, we consider three different schemes for comparison as follows. (i) Joint optimization of power and location with initial association (JOPL): Users associating to the BSs based on the initialization scheme and thereafter, the power and location of the ABS are optimized to maximize the network utility, (ii) cluster-based: ABS follows cluster-based deployment as described in [34] and optimal power is allocated to maximize the network utility, and (iii) Circle-based: A geometric disc problem as described in [35], that aims to minimize the radius of the circle required to cover a specified set of users followed by the optimal power allocation subproblem. Note that, in this scheme, the number of circles must be equal to the number of

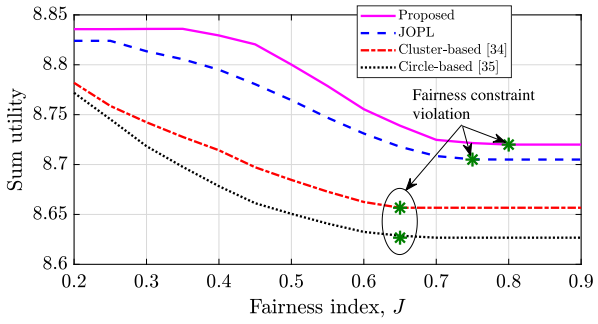

(a)

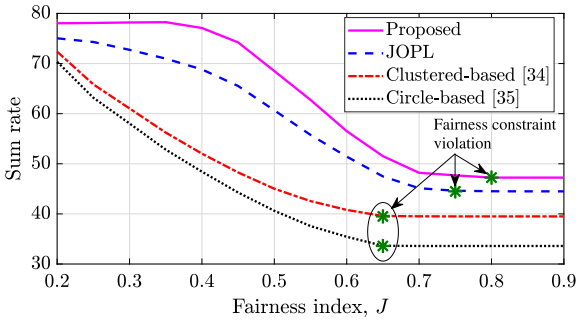

(b)

FIGURE 10. Performance comparison of the proposed scheme with the other schemes when fairness index is varied (a) sum utility and (b) sum rate achieved.

ABS. For all the schemes, we also consider fairness index constraints to have a fair comparison between different schemes.

Fig. 10(a) and (b) are plotted to show the difference in the network utility and sum rate achieved for different schemes while varying the fairness index. It can be observed that for all the schemes, as the fairness index increases, the network utility decreases and finally converges to a certain value. This convergence is observed because the network can only achieve a particular fairness value depending on the user's distribution and the number of RBs.

Furthermore, the joint optimization of association, resources, and multi-ABS location in our proposed scheme results in performance enhancement with respect to the benchmark schemes due to the following reasons. First, the JOPL assumes the users to be associated as described in the initialization scheme, which restricts the optimizer from finding the optimal location and power. Second, cluster-based deployment performs poorly because the cluster-based deployment considers the ABS deployed based on the distance between the ABSs and the users, which restricts the ABS from maximizing the network utility since the ABS is deployed at the centroid location. The circle-based placement performs worse even compared to the cluster-based placement because the cluster-based placement adapts to the non-uniform distribution of users more effectively than a circular placement. Circle-based placement, on the other hand, is best suited for uniform distribution, and where the number of UAVs is

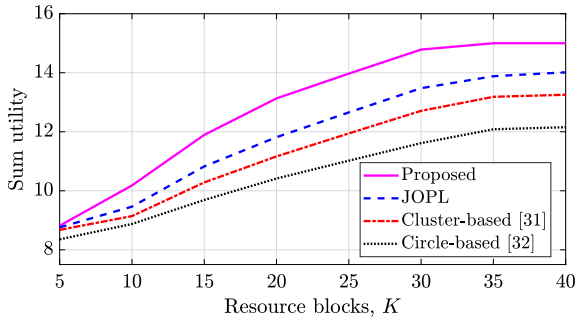

FIGURE 11. Performance comparison of the proposed scheme with the other schemes when the number of RB, K is varied.

undefined. As a result, the clustering-based initialization is more effective than the circle-based initialization. Moreover, our proposed scheme also supports dual-connectivity, where the user can either connect to GBS or/and ABS depending on the channel conditions. In contrast, in the other schemes, the users present in the non-occupying GBS region and GBS occupying region connect to ABSs, and GBS, respectively. This flexibility in the connectivity also results in performance enhancement. Overall, our proposed scheme provides an average of 25% improvement over the benchmark schemes.

Finally, in Fig. 11, we show the variation of network utility with the number of RBs. Fig. 11 is plotted for the same system setup described in Fig. 5 when the fairness index J is set to 0.5. For the proposed scheme, with the increase in the number of RBs, the network utility first increases and then converges to a maximum. This is because, as the RBs increase, more users can be served in different RBs. Thus, even for $J = 0.5$, the optimizer converges to a solution with $J = 0.99$ to return the maximum utility when K is increased. Whereas, for other schemes, the network utility does not reach the maximum value and converges to a particular value, indicating that not all the ground users can be accommodated in the prescribed network settings.

Remark 2: In this paper, we consider omnidirectional antennas at both the ABS and GBS; however, the same approach can be applied, mutatis mutandis, to scenarios involving directional antennas at the ABSs and GBSs. Although the absolute performance metrics may change with the use of directional or multiple antennas, the relative performance trends and the fundamental insights from our analysis are expected to remain consistent.

VII. CONCLUSION

In this paper, we studied an ABS-aided terrestrial communication system, where multiple ABSs are deployed to assist the terrestrial network and expand the coverage range of the system while considering the co-channel interference. We aim to maximize the network utility while also considering the fairness among the users distributed in the network to jointly optimize the user association, ABS placement, and resource allocation. Service fairness to all ground users is ensured

by constraining the utility maximization problem with Jain's fairness metric. The formulated problem is non-convex and an efficient heuristic approach followed by an interference-aware iterative scheme is proposed based on the successive convex approximation method to solve the optimization problem. Numerical results show that the proposed scheme has the flexibility of dual-connectivity and the number of users served by the network increases as we increase the fairness index, showing the coverage capacity of the network. In particular, our proposed scheme gains 25% improvement over the benchmark schemes. Future extensions will explore a distributed approach, where each UAV independently manages its coverage and adapts to mobile users, ensuring continuous communication and coordination to avoid interference.

APPENDIX A
PROOF OF LEMMA 1

We first introduce the variable $\beta^k_{u,m}$ such that (21) is written as

$$b^k_{u,m}(\|\mathbf{q}_m - \mathbf{w}_u\|^2 + z_m^2) \leq \beta^k_{u,m}, \tag{30}$$

where $\beta^k_{u,m} \leq (1-\kappa)\mathcal{P}^L_{u,m} + \kappa$. To make it more simpler, we introduce $0 \leq y^k_{u,m} \leq \mathcal{P}^L_{u,m}$, such that we have

$$\beta^k_{u,m} \leq (1-\kappa) y^k_{u,m} + \kappa, \tag{31}$$

However, the main difficulty lies in handling $\mathcal{P}^L_{u,m}$, which is defined as

$$\mathcal{P}^L_{u,m} = \left(1 + c_1 \exp\left(-c_2\left[\tan^{-1}\left(\frac{z_m}{\|\mathbf{q}_m - \mathbf{w}_u\|}\right) - c_1\right]\right)\right)^{-1}.$$

Then taking

$$\Theta^k_{u,m} = \frac{z_m}{\|\mathbf{q}_m - \mathbf{w}_u\|}, \tag{32}$$

$\mathcal{P}^L_{u,m}$ can be written as $\mathcal{P}^L_{u,m} = (1 + c_1 \exp(-c_2[\tan^{-1}\Theta^k_{u,m} - c_1]))^{-1}$. Thereafter, substituting the obtained $\mathcal{P}^L_{u,m}$ in $y^k_{u,m}$, we get

$$\left(1 + c_1 \exp\left(-c_2[\tan^{-1}\Theta^k_{u,m} - c_1]\right)\right) \leq \frac{1}{y^k_{u,m}} \tag{33}$$

$$y_{k,m} \geq 0. \tag{34}$$

As a result, the constraint (21) can now be equivalently written by (30), (31), (32), (33), and (34).

APPENDIX B
PROOF OF LEMMA 2

The constraint in (32) can be alternatively written as $\Theta^k_{u,m} \leq \frac{z_m}{\|\mathbf{q}_m - \mathbf{w}_u\|}$, which can be readily transformed using the sum of square formulae to represent it in the difference of convex functions given as

$$\frac{1}{2}\left(\Theta^k_{u,m} + \|\mathbf{q}_m - \mathbf{w}_u\|\right)^2 - \frac{1}{2}\left((\Theta^k_{u,m})^2 + \|\mathbf{q}_m - \mathbf{w}_u\|^2\right) \leq z_m. \tag{35}$$

as a property of difference of convex functions, we can write the first order Taylor expansion of the second term of the above inequality, then we get

$$\lambda^k_{u,m} = \frac{1}{2}\left((\Theta^{k,r}_{u,m})^2 + \|\mathbf{q}^r_m - \mathbf{w}_u\|^2\right) + \Theta^{k,r}_{u,m}\left(\Theta^k_{u,m} - \Theta^{k,r}_{u,m}\right) + \|\mathbf{q}^r_m - \mathbf{w}_u\|\left(\|\mathbf{q}_m - \mathbf{w}_u\| - \|\mathbf{q}^r_m - \mathbf{w}_u\|\right), \tag{36}$$

where $\Theta^{k,r}_{u,m}$, $\mathbf{q}^r_m$ are the values of $\Theta^k_{u,m}$, $\mathbf{q}_m$ at the r^{th}-iteration. Using (36) and (35), we get the approximated convex constraint (23).

REFERENCES

[1] Y. Zeng, R. Zhang, and T. J. Lim, "Wireless communications with unmanned aerial vehicles: Opportunities and challenges," *IEEE Commun. Mag.*, vol. 54, no. 5, pp. 36–42, May 2016.

[2] M. Mozaffari, W. Saad, M. Bennis, and M. Debbah, "Efficient deployment of multiple unmanned aerial vehicles for optimal wireless coverage," *IEEE Commun. Lett.*, vol. 20, no. 8, pp. 1647–1650, Aug. 2016.

[3] Y. Zeng, R. Zhang, and T. J. Lim, "Wireless communications with unmanned aerial vehicles: Opportunities and challenges," *IEEE Commun. Mag.*, vol. 54, no. 5, pp. 36–42, May 2016.

[4] L. Zhou, X. Chen, M. Hong, S. Jin, and Q. Shi, "Efficient resource allocation for multi-UAV communication against adjacent and co-channel interference," *IEEE Trans. Veh. Technol.*, vol. 70, no. 10, pp. 10222–10235, Oct. 2021.

[5] H. Wu, X. Tao, N. Zhang, and X. Shen, "Cooperative UAV cluster-assisted terrestrial cellular networks for ubiquitous coverage," *IEEE J. Sel. Areas Commun.*, vol. 36, no. 9, pp. 2045–2058, Sep. 2018.

[6] Z. Wang and J. Zheng, "Performance modeling and analysis of base station cooperation for cellular-connected UAV networks," *IEEE Trans. Veh. Technol.*, vol. 71, no. 2, pp. 1807–1819, Feb. 2022.

[7] Z. Wang, L. Duan, and R. Zhang, "Adaptive deployment for UAV-aided communication networks," *IEEE Trans. Wireless Commun.*, vol. 18, no. 9, pp. 4531–4543, Sep. 2019.

[8] N. Gupta, S. Agarwal, and D. Mishra, "Trajectory design for throughput maximization in UAV-assisted communication system," *IEEE Trans. Green Commun. Netw.*, vol. 5, no. 3, pp. 1319–1332, Sep. 2021.

[9] J. Luo, J. Song, F.-C. Zheng, L. Gao, and T. Wang, "User-centric UAV deployment and content placement in cache-enabled multi-UAV networks," *IEEE Trans. Veh. Technol.*, vol. 71, no. 5, pp. 5656–5660, May 2022.

[10] Y. Zhou, X. Ma, S. Hu, D. Zhou, N. Cheng, and N. Lu, "QoE-driven adaptive deployment strategy of multi-UAV networks based on hybrid deep reinforcement learning," *IEEE Internet Things J.*, vol. 9, no. 8, pp. 5868–5881, Apr. 2022.

[11] I. Valiulahi and C. Masouros, "Multi-UAV deployment for throughput maximization in the presence of co-channel interference," *IEEE Internet Things J.*, vol. 8, no. 5, pp. 3605–3618, Mar. 2021.

[12] L. Wang, H. Zhang, S. Guo, and D. Yuan, "Deployment and association of multiple UAVs in UAV-assisted cellular networks with the knowledge of statistical user position," *IEEE Trans. Wireless Commun.*, vol. 21, no. 8, pp. 6553–6567, Aug. 2022.

[13] C. C. Lai, A. H. Tsai, C. W. Ting, K. H. Lin, J. C. Ling, and C. E. Tsai, "Interference-aware deployment for maximizing user satisfaction in multi-UAV wireless networks," *IEEE Wireless Commun. Lett.*, vol. 12, no. 7, pp. 1189–1193, Jul. 2023.

[14] M. D. Nguyen, L. B. Le, and A. Girard, "Integrated UAV trajectory control and resource allocation for UAV-based wireless networks with co-channel interference management," *IEEE Internet Things J.*, vol. 9, no. 14, pp. 12754–12769, Jul. 2022.

[15] H. Hu, Z. Chen, F. Zhou, Z. Han, and H. Zhu, "Joint resource and trajectory optimization for heterogeneous-UAVs enabled aerial-ground cooperative computing networks," *IEEE Trans. Veh. Technol.*, vol. 72, no. 7, pp. 8812–8826, Jul. 2023.

[16] Y. Li, S. Xu, Y. Wu, and D. Li, "Network energy-efficiency maximization in UAV-enabled air–ground-integrated deployment," *IEEE Internet Things J.*, vol. 9, no. 15, pp. 13209–13222, Aug. 2022.

[17] X. Liu and T. S. Durrani, "Joint multi-UAV deployments for air–ground integrated networks," *IEEE Aerosp. Electron. Syst. Mag.*, vol. 37, no. 12, pp. 4–12, Dec. 2022.

[18] Y. Su, L. Huang, and M. Liwang, "Joint power control and time allocation for UAV-assisted IoV networks over licensed and unlicensed spectrum," *IEEE Internet Things J.*, vol. 11, no. 1, pp. 1522–1533, Jan. 2024.
[19] W. Mei, Q. Wu, and R. Zhang, "Cellular-connected UAV: Uplink association, power control and interference coordination," in *Proc. IEEE Glob. Commun. Conf.*, 2018, pp. 206–212.
[20] W. Mei and R. Zhang, "Uplink cooperative NOMA for cellular-connected UAV," *IEEE J. Sel. Topics Signal Process.*, vol. 13, no. 3, pp. 644–656, Jun. 2019.
[21] X. Pang et al., "Uplink precoding optimization for NOMA cellular-connected UAV networks," *IEEE Trans. Commun.*, vol. 68, no. 2, pp. 1271–1283, Feb. 2020.
[22] Q. Feng, J. McGeehan, E. Tameh, and A. Nix, "Path loss models for air-to-ground radio channels in urban environments," in *Proc. IEEE 63rd Veh. Technol. Conf.*, Melbourne, Australia, 2006, pp. 2901–2905.
[23] Q. V. Pham and W. J. Hwang, "Network utility maximization-based congestion control over wireless networks: A survey and potential directives," *IEEE Commun. Surveys Tuts.*, vol. 19, no. 2, pp. 1173–1200, Second Quarter 2017.
[24] S. Agarwal, S. De, and J. B. Seo, "Cognitive multihoming: Maximizing network utility over CR-assisted cellular network," in *Proc. IEEE Glob. Commun. Workshops*, San Diego, USA, 2015, pp. 1–6.
[25] M. S. Bazaraa, H. D. Sherali, and C. M. Shetty, *Nonlinear Programming: Theory and Algorithms*. Hoboken, NJ, USA: Wiley, 2013.
[26] P. Q. Viet and D. Romero, "Aerial base station placement: A tutorial introduction," *IEEE Commun. Mag.*, vol. 60, no. 5, pp. 44–49, May 2022.
[27] S. Boyd and L. Vandenberghe, *Convex Optimization*. New York, NY, USA: Cambridge Univ. Press, 2004.
[28] N. Gupta, S. Agarwal, and D. Mishra, "Multi-UAV replacement and trajectory design for coverage continuity," in *Proc. IEEE Int. Conf. Commun.*, Seoul, South Korea, 2022, pp. 1–6.
[29] C. You and R. Zhang, "3D trajectory optimization in Rician fading for UAV-enabled data harvesting," *IEEE Trans. Wireless Commun.*, vol. 18, no. 6, pp. 3192–3207, Jun. 2019.
[30] Q. Wu, Y. Zeng, and R. Zhang, "Joint trajectory and communication design for multi-UAV enabled wireless networks," *IEEE Trans. Wireless Commun.*, vol. 17, no. 3, pp. 2109–2121, Mar. 2018.
[31] H. Zhang, J. Zhang, and K. Long, "Energy efficiency optimization for NOMA UAV network with imperfect CSI," *IEEE J. Sel. Areas Commun.*, vol. 38, no. 12, pp. 2798–2809, Dec. 2020.
[32] H. Holtkamp, G. Auer, V. Giannini, and H. Haas, "A parameterized base station power model," *IEEE Commun. Lett.*, vol. 17, no. 11, pp. 2033–2035, Nov. 2013.
[33] S. Lloyd, "Least squares quantization in PCM," *IEEE Trans. Inf. Theory*, vol. IT-28, no. 2, pp. 129–137, Mar. 1982.
[34] M. D. Nguyen, T. M. Ho, L. B. Le, and A. Girard, "UAV placement and bandwidth allocation for UAV based wireless networks," in *Proc. IEEE Glob. Commun. Conf.*, Waikoloa, HI, USA, 2019, pp. 1–6.
[35] J. Lyu, Y. Zeng, R. Zhang, and T. J. Lim, "Placement optimization of UAV-mounted mobile base stations," *IEEE Commun. Lett.*, vol. 21, no. 3, pp. 604–607, Mar. 2017.

NISHANT GUPTA (Member, IEEE) received the B.Tech. degree in electronics and communication engineering from Chandigarh Engineering College, Mohali, India, in 2015, the M.Tech. degree in electronics and communication from Panjab University, Chandigarh, India, in 2018, and the Ph.D. degree from Indian Institute of Technology Ropar, India, in 2023. He was a Postdoctoral Researcher with the Department of Electrical Engineering, Linköping University, Linköping, Sweden. He is currently an Assistant Professor with CCE Department, LNM Institute of Information Technology, Jaipur, India. His research interests include 5G networks, UAV communications, air-borne networks, and optimization.

SATYAM AGARWAL (Senior Member, IEEE) received the Ph.D. degree in electrical engineering from IIT Delhi, New Delhi, India, in 2016. He was an Assistant Professor with IIT Guwahati. In 2017, he was a Postdoctoral Researcher with the Politecnico di Torino, Turin, Italy. He is currently an Assistant Professor with the Department of Electrical Engineering, IIT Ropar, India. His research interests include the wide areas of wireless communication networks, including next-generation networks, 5G networks and architecture, and air-borne networks.

AYMEN FAKHREDDINE received the Ph.D. and M.Sc. degrees in telematic engineering from the University Carlos III Madrid, Madrid, Spain, the M.Sc. degree in advanced wireless communication systems from CentraleSupélec, Gif-sur-Yvette, France, and the Engineering degree in telecommunications from Institute National Des Postes And Telecommunications (INPT), Rabat, Morocco. He is currently a Principal Investigator with the University of Klagenfurt, Klagenfurt, Austria. He was a Senior Researcher with the Technology Innovation Institute, a Senior Researcher with Lakeside Labs (Austria), Researcher with IMDEA Networks Institute, Leganés, Spain, Visiting Researcher with the Singapore University of Technology and Design, and Research Intern with Nokia Bell Labs, Paris-Saclay, France. His research interests are wireless communications, networking, and localization. He was a Chair of ACM MobiSys DroNet 2024, TPC Co-Chair of the IEEE Globecom Workshop on "cellular UAV and satellite communications" in 2022 and 2023, and TPC Co-Chair of the IEEE ICC 2023 workshop on "integrating UAVs into 5G and beyond". He was the recipient of the Best Paper Award at ACM DroNet 2021 and ESPRIT Grant from FWF - Der Wissenschaftsfonds (Austrian Science Fund).